Proceedings World Geothermal Congress 2015
Melbourne, Australia, 19-25 April 2015

Performance Enhancement by Series Double Cascade-evaporation Organic Rankine Cycle (SDCORC) for Geothermal Power Generation

Tailu Li[a], Qiulin Wang[b], Jialing Zhu[b] , Wencheng Fu[c] and Kaiyong Hu[b]

[a] School of Energy and Safety Engineering, Tianjin Chengjian University, Tianjin 300384, PR China

litl@tcu.edu.cn

[b] Key Laboratory of Efficient Utilization of Low and Medium Grade Energy, MOE, Tianjin University, Tianjin 300072, PR China

zhujl@tju.edu.cn

[c] School of Automation, Tianjin University of Technology, Tianjin 300191, PR China

fuwch@tjut.edu.cn

Keywords: Organic Rankine Cycle, Geothermal Water, Cascade Evaporating, Heat Recovery, Performance Enhancement

ABSTRACT

The organic Rankine cycle (ORC) is a promising technology for heat recovery. The major problem is its low cycle efficiency, and the evaporator is a major contributor to the total irreversible losses. In this paper, the heat source is segmented in two temperature ranges to realize cascade evaporating. The series double cascade-evaporation organic Rankine cycle (SDCORC) was put forward. The objective of this paper is to evaluate the performance enhancement of the SDCORC with a reference to the ORC. The system performances (mass flow rate, evaporating temperature, volumetric flow rate (VFR), net power output, system efficiency, and thermal conductances) for the ORC and SDCORC were simulated and compared using R245fa as the working fluid. The objective function is the ratio of the net power output to the total thermal conductance, reflecting both the system earnings and the cost. The results show that the SDCORC can enhance the net power output, and the growth rate differs with intermediate geothermal water temperature (IGWT) and geothermal water inlet temperature (GWIT). The SDCORC exceeds the ORC and enhances the systematic performance with the GWIT. Optimal IGWT and evaporating temperatures of the SDCORC maximize the net power output. The SDCORC presents excellent systematic performance, which should be popularized in engineering applications.

1. INTRODUCTION

The population boom together with social progress accelerates the energy demand, which is predicted to ascend with 33% by 2020 and 84% by 2035 (U.S. Energy Information Administration, 2011). The electricity price has increased by about 12% over the past decade(U.S. Energy Information Administration, 2011; Eurostat, 2013).. Furthermore, serious environmental issues heavily influence the energy policy. The energy gap has been becoming larger and larger, motivating the technologies for power generation from renewable sources and waste heat recovery. Among the cycles, ORC has been focused on due to its simple cycle configuration, high reliability and flexibility, and convenient maintenance (Bianchi and De Pascale, 2011). The ORC-based plants have successfully been adopted in recovering the geothermal resources (Kanoglu, 2011), solar energy (Quoilin et al, 2011), ocean thermal energy (Sun et al, 2012), and other waste heat from different industries (Zhang et al, 2013).

The ORC has been proven promising in converting low and medium grade heat sources into power, but the thermal efficiency is only 8-12% (DiPippo, 2004). Mago et al. (2008) calculated the exergy destruction in ORC using an exergy wheel. The results show that the evaporator has the highest exergy destruction rate, around 77%. Numerous studies have been carried out to reduce the system irreversible loss, thereby improving the system performance. The correlative publications can be summarized as the cycle configuration improvement. Based on the basic ORC, the regenerative organic Rankine cycle (RORC) has been proposed and analyzed. Mago et al. (2008), Pei et al. (2010), Xi et al. (2013), Roy and Misra(2012), Fernández et al. (2011), Franco (2011), and Li et al. (2013) analyzed the RORC. They found that the RORC can increase the system performance but within a limited extent. RORC not only decreases the thermal load of the condenser, but also reduces the irreversible loss in the evaporator. However, the system performance is improved indeed, but only to a small extent.

On the premise of the minimal temperature difference at the pinch point, the single-evaporating characteristic between the heat source and the working fluid in the evaporator is the major factor in bringing about the system irreversible loss. Kosmadakis et al. (2009) and Kosmadakis et al. (2010), Wang et al. (2012), Liu et al. (2012), Zhang et al. (2013), Shu et al. (2013a, 2013b, 2014), Yang et al. (2014), and Li et al. (2014) analyzed dual-loop ORC, and they found that the dual-loop ORC can enhance the system performance. Mohammadkhani et al. (2014) utilized a gas turbine-modular helium reactor by two ORCs. The results showed that the precooler, the intercooler, and the ORC condensers exhibit the worst exergoeconomic performance. The unit cost of electricity increases with the turbine inlet temperature but decreases as the other above mentioned parameters increase.

Form the above-mentioned references on the ORC, it can be obtained that the two or multi stage ORC can indeed improve the system performance. However, it should be pointed out that the cycle configurations are all parallel systems in essence, which may also generate much irreversibility for the high-stage loop due to the high temperature difference between the heat source and working fluid at the inlet of evaporator for the working fluid side. Moreover, no reference has been found to discuss such a cascade-

evaporating organic Rankine cycle for geothermal power generation driven by the low and medium temperature geothermal resources.

The present paper focuses on the evaluation of the systematic performance improvement of the ORC driven by geothermal water of 90-120℃. The heat source is utilized in two different segmented temperature ranges. The series double cascade-evaporating organic Rankine cycle (SDCORC) are put forward to decrease the irreversible loss, especially in the evaporator, thereby enhancing the systematic performance. R245fa is adopted as the working fluid. The main objective is to compare the system performance for SDCORC and to optimize the system parameters, so such the preferable cycle configuration as well as the optimal parameters can be obtained, with the dimensionless ratio of the exergetic efficiency to the total thermal conductance as the objective function. Moreover, the parameters, the mass flow rate of the working fluid, the optimal evaporating temperature, the optimal IGWT, the volumetric flow ratio (VFR), the net power output, the exergetic efficiency, the thermal conductance, and the objective function of the SDCORC were compared with those of the traditional ORC.

2. SYSTEM DESCRIPTION

The heat source is utilized in segmented temperature ranges. Geothermal water from the production wells flows through the evaporator 1 and evaporator 2 successively. It is identified as a-b-c, shown by red lines from Figs. 1. Geothermal water from the outlet of the evaporator 2 will be reinjected. The cooling water goes into the condenser driven by the cooling water pump, and it can be identified as d-e-d, shown by green lines. The heat source and heat sink in the SDCORC are totally the same. Moreover, the counter-current flow between the heat source and heat sink with the working fluid are adopted.

The SDCORC is subcritical, and R245fa was chosen as the working fluid. Figure 1 shows the schematic diagram and the corresponding T-s diagram of the SDCORC. The SDCORC is almost the same with the basic ORC, and the main difference between them two is that the SDCORC adopts series double cascade-evaporating strategy whereas the basic ORC has only one. The SDCORC consists of a high-pressure evaporator 1, a low-pressure evaporator 2, a high-pressure pump 1, a low-pressure pump 2, an induction turbine, a generator, a condenser, a cooling pump, and a cooling tower. The specific flowchart for the working fluid is as follows: The liquid working fluid from the condenser is first pressurized to flow into evaporator 2 where absorbs heat from geothermal water (process b-c) coming from the evaporator 1 to generate low-pressure saturated or superheated vapour (process 4”-1”). A portion of the saturated liquid at the saturated pressure in the evaporator 2 is pumped to the evaporator 1 to absorb heat from geothermal water (process a-b) coming from production wells to generate high-pressure saturated or superheated vapour (process 4’-1’). The vapour at the state points 1’ and 1” flow into the corresponding stages of the induction turbine where its enthalpy is converted into mechanical energy to drive the generator to produce electricity (process 1’ (1”)-2). The discharging steam from the turbine outlet is led to the condenser where it is liquefied by the cooling water (process 2-3). The liquid available at the condenser outlet divides into two parts pressurized by the pumps 1 and 2, and then another new cycle begins. The PDCORC can be identified as 1’(1”)-2-3-4’(4”)-1’(1”), shown by green lines.

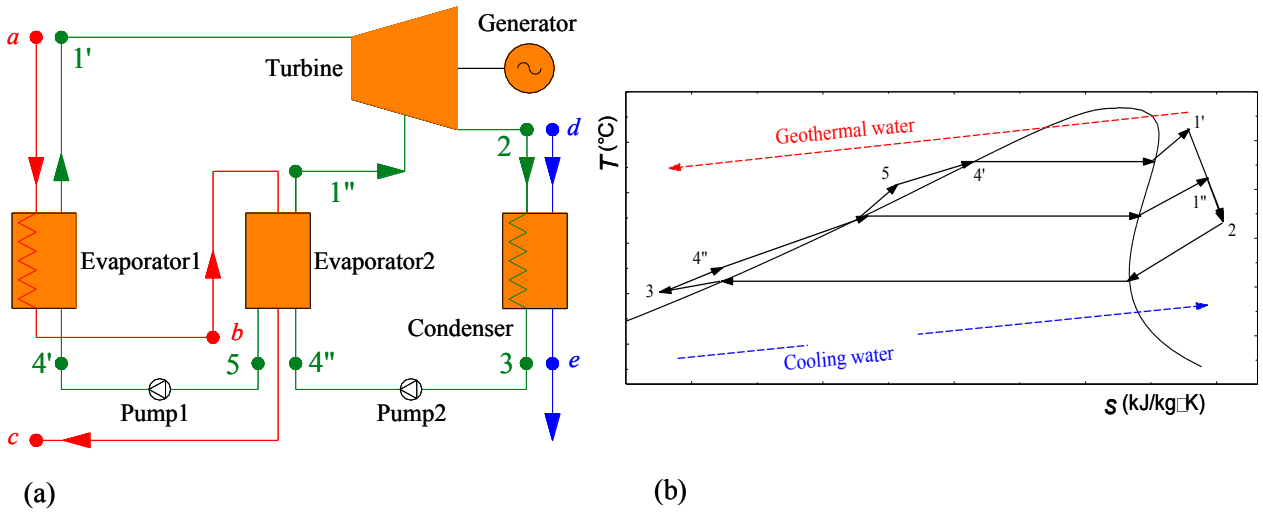

Figure 1: Schematic diagram (a) and *T-s* diagram of the SDCORC.

3. MATHEMATICAL MODELLING

The energetic and exergetic analysis based on the first and second laws of thermodynamics were carried out for the working fluid investigated. For simplicity, the following hypotheses were made:

(1) Geothermal power plants operate in a steady-state condition.

(2) Superheated vapour is considered at the outlet of the evaporator, with a degree of superheat of 5℃. Saturated liquid is considered at the condenser exit.

(3) The working fluid at the inlet of the evaporator 1 for SDCORC is considered at the saturated pressure in the evaporator 2.

(4) Pressure drops throughout the evaporator, the condenser and the pipelines are negligible.

(5) The kinetic and potential energy changes are negligible.

(6) The temperature and friction losses are negligible.

(7) Energy loss during the mixing process of the high- and low-pressure vapour in the turbine is negligible.

The mathematical model for PDCORC is expressed by the following equations:

Turbine:

$$\eta_t=(h_{1'}-h_2)/(h_{1'}-h_{2s})=(h_{1''}-h_2)/(h_{1''}-h_{2s}) \tag{1}$$

where η and h denote the efficiency and the enthalpy, respectively; the subscript t stands for the turbine, and s means the isentropic process.

$$W_t=(m_{wf,1}(h_{1'}-h_{2s})+m_{wf,2}(h_{1''}-h_{2s}))\eta_t \tag{2}$$

$$m_{wf,1}=\begin{cases}\dfrac{m_{gw}c_{p,gw}(T_{gw,in}-T_{gw,mid})}{h_{1'}-h_{4'}},(T_{eva,1}\le T_{eva,1,opt})\\ \dfrac{m_{gw}c_{p,gw}(T_{gw,in}-\Delta T_{pp}-T_{eva,1})}{h_{1'}-h_{4'}},(T_{eva,1}\ge T_{eva,1,opt})\end{cases} \tag{3}$$

$$m_{wf,2}=\begin{cases}\dfrac{m_{gw}c_{p,gw}(T_{gw,mid}-T_{gw,out})}{h_{1''}-h_{4''}}-m_{wf,1},(T_{eva,2}\le T_{eva,2,opt})\\ \dfrac{m_{gw}c_{p,gw}(T_{gw,mid}-\Delta T_{pp}-T_{eva,2})}{h_{1''}-h_{4''}},(T_{eva,2}\ge T_{eva,2,opt})\end{cases} \tag{4}$$

where W and m represent the power output and the mass flow rate, respectively; the subscript wf stands for the working fluid.

$$I_t=T_0(m_{wf,1}(s_2-s_{1'})+m_{wf,2}(s_2-s_{1''})) \tag{5}$$

where I and s stand for the irreversible loss and the entropy, respectively; T_0 means the ambient temperature.

Condenser:

$$Q_c=(m_{wf,1}+m_{wf,2})(h_2-h_3) \tag{6}$$

where Q stands for the thermal load; the subscript c stands for condenser.

$$I_c=(m_{wf,1}+m_{wf,2})T_0[(s_3-s_2)-(h_3-h_2)/T_L] \tag{7}$$

where T stands for the temperature; T_L stands for the average temperature of the cooling water.

$$W_{p,cw}=m_{cw}\Delta P_{cw}/(\eta_{p,cw}\rho_{cw}) \tag{8}$$

where ρ means for the density; the subscript p stands for the pump; ΔP_{cw} represents the pressure loss in the cooling water circuit; the subscript cw stands for the cooling water.

$$(KA)_{c,pre}=Q_{c,pre}/(\Delta T_{c,pre}) \tag{9}$$

$$(KA)_{c,con}=Q_{c,con}/(\Delta T_{c,con}) \tag{10}$$

$$(KA)_{c,total}=(KA)_{c,pre}+(KA)_{c,con} \tag{11}$$

$$Q_c=Q_{c,pre}+Q_{c,con} \tag{12}$$

where K and A stand for the heat transfer coefficient and the area, respectively; the subscripts pre, and con stands for the pre-cooling and condensing.

Pump 1:

$$\eta_{p1}=(h_{4',s}-h_5)/(h_{4'}-h_5) \tag{13}$$

where the subscript 5 stands for the saturated liquid at the saturated temperature in the evaporator 2.

$$W_{p1}=m_{wf,1}(P_{e'}-P_{e''})/(\eta_{p1}\rho_{wf}) \tag{14}$$

$$I_{p1}=m_{wf,1}T_0(s_{4'}-s_5) \quad (15)$$

Pump 2:

$$\eta_{p2}=(h_{4'',s}-h_3)/(h_{4''}-h_3) \quad (16)$$

$$W_{p2}=(m_{wf,1}+m_{wf,2})(P_{e''}-P_c)/(\eta_{p2}\rho_{wf}) \quad (17)$$

$$I_{p2}=(m_{wf,1}+m_{wf,2})T_0(s_{4''}-s_3) \quad (18)$$

Evaporator 1:

$$Q_{e1}=m_{wf,1}(h_{1'}-h_{4'}) \quad (19)$$

where the subscripts e1 and wf1 stand for the evaporator 1 and the working fluid evaporated in the evaporator 1.

$$I_{e1}=m_{wf,1}T_0[(s_{1'}-s_{4'})-(h_{1'}-h_{4'})/T_{H'}] \quad (20)$$

where $T_{H'}$ represents the average temperature of the heat source in the evaporator 1.

$$W_{p,gw1}=m_{gw}\Delta P_{gw1}/(\eta_{p,gw}\rho_{gw}) \quad (21)$$

where gw represents geothermal water; ΔP_{gw1} stands for the pressure drop in the evaporator 1.

$$(KA)_{e1,pre}=Q_{e1,pre}/(\Delta T_{e1,pre}) \quad (22)$$

$$(KA)_{e1,eva}=Q_{e1,eva}/(\Delta T_{e1,eva}) \quad (23)$$

$$(KA)_{e1,sup}=Q_{e1,sup}/(\Delta T_{e1,sup}) \quad (24)$$

$$(KA)_{e1,total}=(KA)_{e1,pre}+(KA)_{e1,eva}+(KA)_{e1,sup} \quad (25)$$

$$Q_{e1}=Q_{e1,pre}+Q_{e1,eva}+Q_{e1,sup} \quad (26)$$

where the subscript e1 represents the evaporator 1; the subscripts pre, eva, and sup stands for the pre-heating, evaporating, and superheating.

Evaporator 2:

$$Q_{e2}=m_{wf,1}(h_5-h_{4''})+m_{wf,2}(h_{1''}-h_{4''}) \quad (27)$$

$$I_{e2}=m_{wf,2}T_0[(s_{1''}-s_{4''})-(h_{1''}-h_{4''})/T_{H''}] \quad (28)$$

where the subscripts e2 and wf2 stand for the evaporator 2 and the working fluid evaporated in the evaporator 2; $T_{H''}$ represents the average temperature of the heat source in the evaporator 2.

$$W_{p,gw2}=m_{gw}\Delta P_{gw2}/(\eta_{p,gw}\rho_{gw}) \quad (29)$$

where ΔP_{gw1} stands for the pressure drop in the evaporator 2.

$$(KA)_{e2,pre}=Q_{e2,pre}/(\Delta T_{e2,pre}) \quad (30)$$

$$(KA)_{e2,eva}=Q_{e2,eva}/(\Delta T_{e2,eva}) \quad (31)$$

$$(KA)_{e2,sup}=Q_{e2,sup}/(\Delta T_{e2,sup}) \quad (32)$$

$$(KA)_{e2,total}=(KA)_{e2,pre}+(KA)_{e2,eva}+(KA)_{e2,sup} \quad (33)$$

$$Q_{e2}=Q_{e2,pre}+Q_{e2,eva}+Q_{e2,sup} \quad (34)$$

where the subscripts e stands for the evaporator.

Total thermal conductance in the evaporator:

$$(KA)_e=(KA)_{e1}+(KA)_{e2} \quad (35)$$

Total thermal conductance:

$$(KA)_{total}=(KA)_e+(KA)_c \quad (36)$$

Total irreversibility:

$$I_{total}=I_t+I_c+I_{p1}+I_{p2}+I_{e1}+I_{e2}=T_0[m_{wf,1}((h_{4'}-h_{1'})/T_{H'}+(h_2-h_3)/T_L)+m_{wf,2}((h_{4''}-h_{1''})/T_{H''}+(h_2-h_3)/T_L)] \quad (37)$$

Net power output:

$$W_{net}=\eta_m\eta_g W_t-W_{p1}-W_{p2}-W_{p,cw}-W_{p,gw} \quad (38)$$

where η_m and η_g are the conversion efficiency of the mechanical energy and the efficiency of the generator, respectively.

Thermal efficiency:

$$\eta_{th}=W_{net}/(Q_{e1}+Q_{e2}) \quad (39)$$

The exergy for geothermal water at the inlet and outlet of the evaporator can be expressed as:

$$m_{gw}(h_a-h_c)=m_{wf,1}(h_{1'}-h_{4'})+m_{wf,1}(h_5-h_{4''})+m_{wf,2}(h_{1''}-h_{4''}) \quad (40)$$

where the subscripts a and c stand for the state points of geothermal water.

$$Ex_{gw}=m_{gw}[(h_a-h_c)-T_0(s_a-s_c)] \quad (41)$$

Exergetic efficiency:

$$\eta_{ex}=W_{net}/Ex_{gw} \quad (42)$$

Objective function:

$$f_{obj}=\eta_{ex}/(KA)_{total} \quad (43)$$

3. VALIDATION

Numerical solution is validated by the data of Saleh et al. (2007) for various working fluids-based ORC without regenerator and for the same operating conditions. The results of present solutions showed a very good agreement with the results in the Reference, as shown in Table 1. The highest absolute difference in the thermal efficiency is only 0.26%, with the highest relative difference of 3.48%. The differences mainly arise from the selection of equation of state, and the BACKONE equation of state was adopted in the Reference while the fundamental equation of state was selected in this paper.

Table 1 Validation of the numerical model with previous published data for various fluids-based ORC

Substances	t_{cri} ,℃	t_1 ,℃	t_3 ,℃	P_e ,MPa	P_c ,MPa	V_1 ,m^3/s	VFR	η_{th},%	Sources
R125	66.18	40.06	30.00	2.000	1.564	2.878	1.270	2.32	Saleh et al. ,2007
R125	66.18	40.06	30.00	2.000	1.564	2.834	1.360	2.35	Present
R290	96.65	57.14	30.00	2.000	1.079	1.063	1.667	5.91	Saleh et al. ,2007
R290	96.65	57.14	30.00	2.000	1.079	1.049	1.764	5.81	Present
R134a	101.03	67.75	30.00	2.000	0.772	0.656	2.357	7.74	Saleh et al. ,2007
R134a	101.03	67.75	30.00	2.000	0.772	0.639	2.483	7.48	Present

4. RESULTS AND DISCUSSION

This study takes the subcritical ORC based on geothermal water as an example for low- and medium-grade heat source recovery. Table 2 shows the system parameters including the ORC, heat source, and heat sink, which is extracted from an existed practical ORC-based geothermal power plant in China. GWIT is varied at steps of 5℃ in the range of 90-120℃, however, geothermal water outlet temperature is confined to be no lower than 70℃ to prevent silica precipitation in the rejection wells (Toffolo et al., 2014). R245fa is selected and used for the working fluid, and its main physical properties are shown in Table 3, which was previously screened as among broad candidates because of its excellent performance in the low- to medium-temperature range (Li et al. 2014, Li et al. 2012, Li et al. 2013, Li et al. 2013, Li et al. 2013, Shengjun et al. 2011, Fiaschi et al. 2012). There are C, H, and F atoms in the molecular formula, so such it belongs to HFC substances whose ozone depletion potential (ODP) is zero. Moreover, R245fa is non-flammable.

Table 2 Simulation parameters and boundary conditions used in this study.

Parameter	Value	Parameter	Value
GWIT (℃)	90-120	Turbine isentropic efficiency (%)	75
Tail water outlet temperature (℃)	≥70	Pump isentropic efficiency (%)	60
Geothermal water flow rate (m^3/h)	69.45	Cooling pump efficiency (%)	75
Cooling water inlet temperature (℃)	25	Mechanical efficiency (%)	97

Cooling water outlet temperature (℃)	35	Generator efficiency (%)	98
Pinch point temperature difference (℃)	5	Environmental temperature(℃)	25
Turbine inlet superheated degree (℃)	5	Environmental pressure (MPa)	0.101325

Table 3 Thermodynamic properties of R245fa

Substance	Physical data				Environmental data			Source
	M(g/mol)	T_b(℃)	T_{cri}(℃)	P_{cri}(MPa)	ALT(yr)	ODP	GWP(100yr)	
R245fa	134.05	14.90	154.05	3.640	7.6	0	1030	(Calm and Hourahan, 2007)

Table 4 lists the effect of the evaporating temperature ($T_{eva,ORC}$) of the ORC on mass flow rate (m_{wf}), volumetric flow ratio (VFR), and Jakob number (Ja) at $T_{gw,in}$=100℃. Clearly, as indicated in the table, VFR is proportional to T_{eva}. For a given ambient condition, the system condensing pressure can be regarded as a constant, which implies that the VFR is only determined by $T_{eva,ORC}$, i.e., there is a one-to-one correspondence relationship between VFR and T_{eva}. From Macchi and Perdichizzi (1981), lower VFRs lead to high turbine efficiencies. Moreover, according to Invernizzi et al. (2007), the turbine efficiency can exceed 80% only when the VFR is lower than 50. The highest VFR in this study is only 4.488, thereby manifesting that the turbine efficiency can be relatively high.

The Jakob number (Ja) is the ratio of sensible to latent heat absorbed during liquid-vapor phase change in the evaporator. Apparent, as indicated in the table, Ja exhibits the similar variation trend with VFR, and it is mainly dependent on $T_{eva,ORC}$ once the ambient conditions are fixed. It should be pointed out that the specific enthalpy at the evaporator inlet are slightly different with T_{eva} and is proportional to T_{eva}, however, the difference can be ignored due to the low range of $T_{eva,ORC}$. The increase in $T_{eva,ORC}$ leads to the increasing of the sensible heat and the reduction of the latent heat during liquid-vapor phase change in the evaporator, as shown in Figure1(b).

Based on the first law of thermodynamics, m_{wf} is associated with the thermal load in the evaporator and the specific enthalpy change of the working fluid. From Table 3, m_{wf} decreases with $T_{eva,ORC}$, and the change rate $\partial m_{wf} / \partial T_{eva,ORC}$ is associated with $T_{eva,ORC}$. There exists an optimal evaporating temperature $T_{eva,ORC,opt}$ mutating $\partial m_{wf} / \partial T_{eva,ORC}$, i.e., as a whole, $\partial(m_{wf} / m_{wf,max}) / \partial T_{eva}$ for $T_{eva,ORC} \le T_{eva,ORC,opt}$ and $T_{eva,ORC} \ge T_{eva,ORC,opt}$ can be regarded as fixed, and the absolute value of $\partial(m_{wf} / m_{wf,max}) / \partial T_{eva,ORC}$ for $T_{eva,ORC} \le T_{eva,ORC,opt}$ is much lower than that for $T_{eva,ORC} \ge T_{eva,ORC,opt}$. This is due to that the increasing of T_{eva} enhances the specific enthalpy rise in the evaporator. On the other hand, a higher $T_{eva,ORC}$ sharply reduces the available heat to vaporize the working fluid. Moreover, it should be pointed out from Eqs. (3), and (4) that the available heat are totally the same for $T_{eva,ORC} \le T_{eva,ORC,opt}$ at the given $T_{gw,in}$, therefore, m_{wf} mainly relied on $T_{eva,ORC}$. For $T_{eva,ORC} \ge T_{eva,ORC,opt}$, the available heat is inversely proportional to $T_{eva,ORC}$, and this is due to the increase of $T_{gw,out}$. Increasing T_{eva} corresponds with decreasing the available heat to vaporize the working fluid, the two parameters integrate with each other, making a significant reduction of the working fluid for $T_{eva,ORC} \ge T_{eva,ORC,opt}$.

Table 4 Effect of evaporating temperature on system parameters of ORC at $T_{gw,in}$=100℃.

T_{eva} (℃)	VFR	m_{wf} (kg/s)	Ja	T_{eva} (℃)	VFR	m_{wf} (kg/s)	Ja
65	3.034	40.23	0.3386	80	4.611	29.05	0.5089
66	3.123	40.1	0.349	81	4.737	27.26	0.5216
67	3.213	39.98	0.3595	82	4.866	25.46	0.5344
68	3.306	39.85	0.3701	83	4.998	23.64	0.5474
69	3.402	39.72	0.3809	84	5.133	21.79	0.5607
70	3.499	39.6	0.3918	85	5.271	19.93	0.5741
71	3.599	39.48	0.4028	86	5.412	18.04	0.5878
72	3.701	39.36	0.414	87	5.557	16.14	0.6016
73	3.806	39.24	0.4253	88	5.705	14.21	0.6157
74	3.913	39.12	0.4368	89	5.856	12.25	0.6301
75	4.022	37.7	0.4484	90	6.011	10.28	0.6446
76	4.135	36	0.4601	91	6.169	8.275	0.6595
77	4.25	34.29	0.4721	92	6.331	6.247	0.6746
78	4.367	32.56	0.4842	93	6.497	4.193	0.6899
79	4.488	30.81	0.4965	94	6.666	2.111	0.7056

Figure 2 shows the effect of the evaporating temperature (T_{eva}) on the thermal conductance in the condenser ($(KA)_{con}$) and evaporator ($(KA)_{eva}$) at $T_{gw,in}$=100℃.Clearly, as indicated in the figure, $(KA)_{con}$ decreases with T_{eva}, and ($\partial((KA)_{con})/\partial T_{eva}$) at different with T_{eva}. $\partial((KA)_{con})/\partial T_{eva}$ can be approximately regarded as constant for $T_{eva} \le T_{eva,opt}$ and $T_{eva} \ge T_{eva,opt}$. Moreover, $\partial((KA)_{con})/\partial T_{eva}$ for $T_{eva} \le T_{eva,opt}$ is higher than that for $T_{eva} \ge T_{eva,opt}$. $(KA)_{con}$ is determined by the thermal load in the condenser (Q_c) and the log mean temperature difference in the condenser (ΔT_{con}). For $T_{eva} \le T_{eva,opt}$, Q_c is always decreasing due to that Q_c is constant at this time whereas W_{net} is increasing, on the other hand, an increase in T_{eva} leads to an increase in the temperature of the working fluid at the turbine outlet, thereby increasing ΔT_{con}. For $T_{eva} \ge T_{eva,opt}$, Q_c is sharply declined due to the increasing of $T_{gw,out}$, moreover, ΔT_{con} becomes larger and larger.

Compared with $(KA)_{con}$, $(KA)_{eva}$ presents distinct variation trend for $T_{eva} \le T_{eva,opt}$ and $T_{eva} \ge T_{eva,opt}$, and $(KA)_{eva}$ is dependent on (Q_e) and the log mean temperature difference in the condenser (ΔT_{eva}), and it gets the maximal value at $T_{eva} = T_{eva,opt}$. For $T_{eva} \le T_{eva,opt}$, Q_e is always constant whereas ΔT_{eva} is decreased with the increase of T_{eva}, thereby the parameter $\partial((KA)_{eva})/\partial T_{eva}$ is positive. However, For $T_{eva} \le T_{eva,opt}$, Q_e is sharply declined and ΔT_{eva} is always decreased with the increase of T_{eva}, but the influence of Q_e to T_{eva} is more dramatic compared with ΔT_{eva}, thereby leading to a negative $\partial((KA)_{eva})/\partial T_{eva}$.

The total thermal conductance in the evaporator ($(KA)_{total}$) with the evaporating temperature (T_{eva}) at $T_{gw,in}$=100℃ is presented in Figure2. Apparently, as shown in the figure, $(KA)_{total}$ exhibits the similar variation trend with $(KA)_{con}$, i.e., $(KA)_{total}$ decreases with T_{eva}, but the change rate ($\partial((KA)_{con})/\partial T_{eva}$) at different evaporating temperature are different. The rate $\partial((KA)_{total})/\partial T_{eva}$ can be approximately regarded as constant for $T_{eva} \le T_{eva,opt}$ and $T_{eva} \ge T_{eva,opt}$, coincidently, $\partial((KA)_{total})/\partial T_{eva}$ for $T_{gw,in}$ investigated in this paper are almost the same. Moreover, $\partial((KA)_{total})/\partial T_{eva}$ for $T_{eva} \le T_{eva,opt}$ is higher than that for $T_{eva} \ge T_{eva,opt}$. From Eq. (36), $(KA)_{total}$ is determined by $(KA)_{con}$ and $(KA)_{eva}$. $(KA)_{con}$ is much higher than $(KA)_{eva}$ due to the pretty smaller temperature difference in the condenser. So $(KA)_{total}$ is dependent on $(KA)_{con}$, and this is the reason why $(KA)_{total}$ and $(KA)_{con}$ presented the similar variation rules. For $T_{eva} \ge T_{eva,opt}$, compared with ΔT_{con} and ΔT_{eva}, Q_c and Q_c are both sharply declined due to the increasing of $T_{gw,out}$, i.e., the evident decrease in the thermal load is a main contributor the $(KA)_{total}$.

The net power output (W_{net}) at different evaporating temperature (T_{eva}) at $T_{gw,in}$=100℃ is also presented in Figure2. Evidently, as shown in the figure, W_{net} first increases until achieving the maximal value at $T_{eva,opt}$ and then decreases with T_{eva}. Furthermore, $W_{net,max}$ at $T_{gw,in}$=100℃ is 622.7kW. The change rate $\partial W_{net}/\partial T_{eva}$ is proportional to T_{eva}, which manifests that $T_{gw,in}$ can output more power for higher $T_{gw,in}$ due to the more available energy provision.

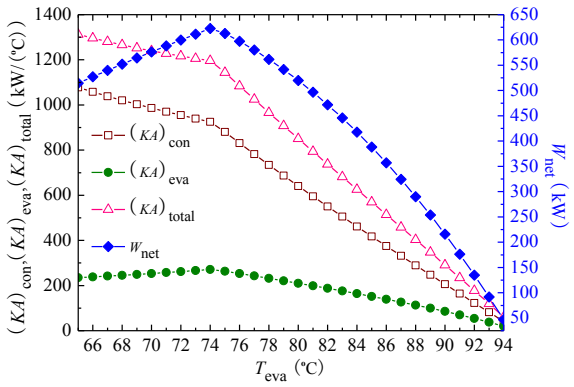

Figure 2: Thermal conductance in condenser and evaporator with evaporating temperature at $T_{gw,in}$=100℃

Figure 3 shows the thermal efficiency (η_{th}) and the exergetic efficiency (η_{ex}) with different evaporating temperature (T_{eva}) at $T_{gw,in}$=100℃. Obviously, as shown in the figure, η_{th} is proportional to T_{eva}, and there is one-to-one correspondence between η_{ex} and T_{eva}. In this sense, $T_{gw,in}$ is a decisive factor to η_{th}. However, no such relationship exists between η_{th} and T_{eva}, and the variation trend of η_{ex} is coincident with that of W_{net}. For $T_{eva} \le T_{eva,opt}$, η_{ex} is only relied on W_{net} because geothermal water has the same parameters. On the other hand, for $T_{eva} \ge T_{eva,opt}$, η_{ex} are determined by W_{net} and the exergy at the inlet and outlet of the evaporator for geothermal water, which differs from one working condition to anather. This is due to that W_{net} is a major factor in determining η_{ex}. It is noteworthy that $T_{eva,opt}$ makes η_{ex} achieve the maximal value.

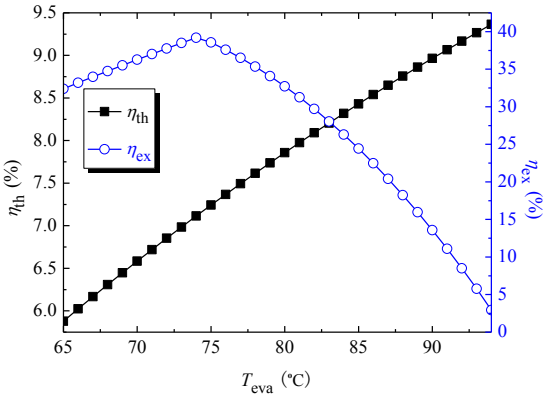

Figure 3: System efficiency and objective function with evaporating temperature at $T_{gw,in}$=100℃.

Table 5 shows the effect of the intermediate geothermal temperature ($T_{gw,mid}$) on mass flow rate (m_{wf}), volumetric flow ratio (VFR), and Jakob number (Ja) at $T_{gw,in}$=100℃. Clearly, as indicated in the table, $T_{gw,mid}$ as well as $T_{eva,1}$ and $T_{eva,2}$ has a decisive effect on the system performance and should be optimized. $T_{eva,1}$ and $T_{eva,2}$ are generally inversely proportional with $T_{gw,mid}$, which is due to that decreasing $T_{gw,mid}$ reduces the average temperature of the heat source in the evaporators, thereby leading to lower $T_{eva,1,opt}$ and $T_{eva,2,opt}$. Moreover, $T_{gw,mid.opt}$ together with $T_{eva,1,opt}$ and $T_{eva,2,opt}$ maximizes the net power output. VFR and Ja depend on the T_{eva}, so the two parameters are no more discussed in detail. $m_{wf,1}$ and $m_{wf,2}$ manifest different variation trends with $T_{gw,mid}$, i.e., $m_{wf,1}$ is inversely proportional to $T_{gw,mid}$, whereas there is proportional relationship between $m_{wf,2}$ and $T_{gw,mid}$. This is because increasing $T_{gw,mid}$ increases the available heat in the high-pressure evaporator and decreases the available heat in the low-pressure evaporator. Furthermore, the total mass flow rate m_{wf} differs with working condition.

Table 5 Effect of evaporating temperature on system parameters of SDCORC at $T_{gw,in}$=100℃.

$T_{gw,mid}$ (℃)	$T_{eva,1}$ (℃)	$T_{eva,2}$ (℃)	$m_{wf,1}$ (kg/s)	$m_{wf,2}$ (kg/s)	VFR_1	VFR_1	Ja_1	Ja_2
99	94	73	1.402	37.42	6.296	3.727	0.2139	0.3615
98	93	73	3.313	35.64	6.11	3.727	0.199	0.3615
97	92	73	4.986	33.85	5.97	3.727	0.1876	0.3615
96	91	73	6.67	32.06	5.832	3.727	0.1765	0.3615
95	90	73	8.366	30.28	5.696	3.727	0.1655	0.3615
94	89	73	10.07	28.49	5.562	3.727	0.1547	0.3615
93	88	73	11.79	26.71	5.431	3.727	0.144	0.3615
92	88	73	13.48	24.92	5.431	3.727	0.144	0.3615
91	87	73	15.21	23.14	5.303	3.727	0.1335	0.3615
90	86	73	16.96	21.36	5.176	3.727	0.1232	0.3615
89	85	73	18.73	19.58	5.052	3.727	0.1129	0.3615
88	84	73	20.5	17.79	4.93	3.727	0.1028	0.3615
87	83	73	22.29	16.01	4.81	3.727	0.0929	0.3615
86	82	73	24.1	14.23	4.692	3.727	0.08308	0.3615
84.89	81	73	25.92	12.45	4.577	3.727	0.07338	0.3615
84.74	81	72	25.97	12.39	4.577	3.63	0.08247	0.3511
83.79	80	72	27.68	10.62	4.463	3.63	0.07285	0.3511
83.66	80	71	27.68	10.57	4.463	3.535	0.08187	0.3409
83.52	80	70	27.68	10.52	4.463	3.441	0.09088	0.3308
83.38	80	69	27.68	10.47	4.463	3.35	0.09986	0.3208
82.43	79	69	29.37	8.726	4.352	3.35	0.09023	0.3208
82.29	79	68	29.37	8.686	4.352	3.26	0.09915	0.3109
82.15	79	67	29.37	8.647	4.352	3.172	0.1081	0.3011
82	79	66	29.37	8.609	4.352	3.087	0.1169	0.2915
81.05	78	66	31.05	6.886	4.243	3.087	0.1073	0.2915
80.9	78	65	31.05	6.858	4.243	3.002	0.1158	0.2823
79.95	77	65	32.71	5.143	4.136	3.002	0.1063	0.2823

The system irreversible loss of ORC, and SDCORC at $T_{gw,in}$=100℃ is shown in Figure 4. The total irreversible loss of the ORC and the SDCORC reduces sequentially, and the irreversible loss in the evaporator manifests a similar variation trend. However, the irreversible loss in the turbine, pump, and condenser for ORC, and SDCORC are increased. For the evaporator, the SDCORC utilizes geothermal water in segmented temperature range, thereby improving the matching between geothermal water and working fluid, so such the irreversible loss in the evaporator declines. A mew parameter, the equivalent evaporating temperature, is used to evaluate the SDCORC, which is expressed as follows:

$$T_{eva,eq} = \frac{m_{wf,1}T_{eva,1} + m_{wf,2}T_{eva,2}}{m_{wf,1} + m_{wf,2}} \tag{44}$$

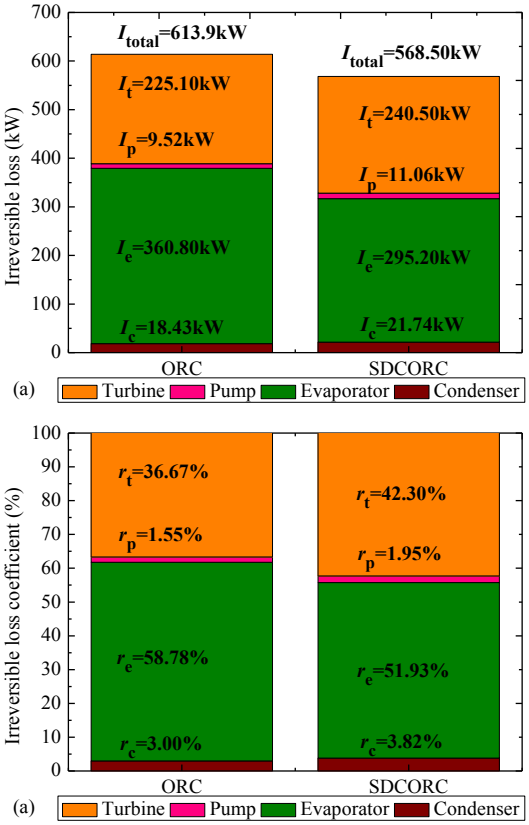

Figure 4: Irreversible loss (a) and irreversible loss coefficient (b) of system component at $T_{gw,in}$=100℃.

For a given turbine efficiency, m_{wf} and VFR are the decisive factors for the irreversible loss caused by the turbine, and the highest difference of the working fluid between SDCORC and ORC is up to 11.01%, so such the irreversible loss caused by the turbine is mainly influenced by the VFR. Moreover, $T_{eva,eq,SDRORC}$ is higher than $T_{eva,ORC}$. This is the reason for more irreversible loss in the turbine for the SDCORC. It should be pointed out that the irreversible loss generated by the pump for the ORC, and SDCORC ascends sequentially, and it is similar with the irreversible loss caused by the turbine. SDCORC shows the highest irreversible loss in the condenser. The working fluid at the outlet of the condenser is set to be 30℃. Furthermore, the working fluid at the inlet of the condenser for the SDCORC has a higher temperature than that for the ORC. Overall, the evaporator contributes the most to the total irreversible loss followed the turbine. However, the condenser only accounts for 3.82% in the SDCORC, this is due to the low log mean temperature difference in it. From the aspect of reducing the irreversible loss in the evaporator and the total irreversible loss, SDCORC is more favourable than ORC.

Figure 5 shows the thermal conductance in the condenser ($(KA)_{con}$) and evaporator ($(KA)_{eva}$) with the intermediate geothermal water temperature ($T_{gw,mid}$) at $T_{gw,in}$=100℃. Obviously, as shown in the figure, $(KA)_{con}$ first decreases until achieving the minimum and then increases with $T_{gw,mid}$, but it is just the opposite for $(KA)_{eva}$). i.e., $(KA)_{eva}$ first increases until achieving the maximum, and then decreases with $T_{gw,mid}$. $(KA)_{con}$ gets the minimal value at $T_{gw,mid}$ =88℃, whereas $(KA)_{eva}$ gets the maximal value at $T_{gw,mid}$ =85℃.

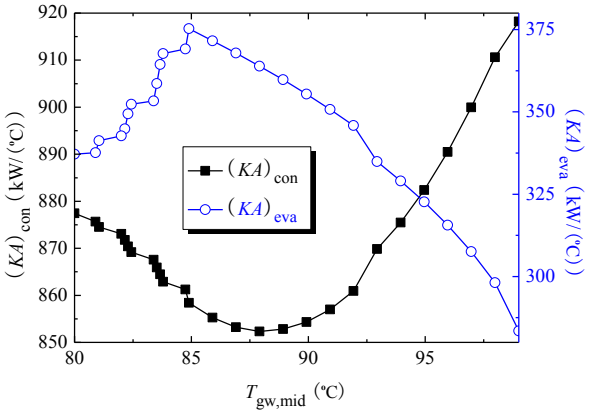

Figure 5: Thermal conductance in condenser and evaporator with intermediate geothermal water temperature at $T_{gw,in}$=100℃.

Figure 6 shows the total thermal conductance ($(KA)_{total}$) and the net power output (W_{net}) with the intermediate geothermal water temperature ($T_{gw,mid}$) at $T_{gw,in}$=100℃. Obviously, as shown in the figure, as $T_{gw,mid}$ increases, $(KA)_{total}$ is first increasing until achieving the maximal value and then it is reduced until obtaining the minimal value, and afterwards it is gradually increased. From Figure 5, $(KA)_{con}$ is much larger than $(KA)_{eva}$ at a fixed $T_{gw,mid}$, indicating that $(KA)_{total}$ is more influenced by $(KA)_{con}$. Moreover, $(KA)_{total}$ exhibits the similar variation trend except for $T_{gw,mid}$ ≥ 94℃. W_{net} is associated with $T_{gw,mid}$, there exists an optimal intermediate geothermal water temperature $T_{gw,mid,opt}$ maximizing the W_{net}. W_{net} achieves its maximal value of 669.7kW at $T_{gw,mid}$ = 88℃, $T_{eva,1,opt}$ = 84℃, and $T_{eva,2,opt}$ = 73℃.

Combining Figs. 2 with 6, it should be pointed out that $T_{gw,mid}$ is a key parameter to the SDCORC, and not all the available $T_{gw,mid}$ can improve the net power output, i.e., the SDCORC can output more power when 80 ≤ $T_{gw,mid}$ ≤ 98℃. The dimensionless ratio $W_{net,max,SDCORC}/W_{net,max,ORC}$ is enhanced by about 7.55%. Furthermore, $(KA)_{total,SDCORC}$ and $(KA)_{total,ORC}$ are almost the same, 1196.40 and 1216.22kW/℃.

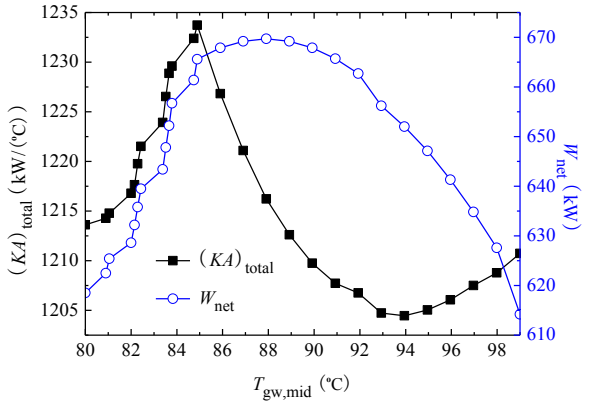

Figure 6: Total thermal conductance and net power output with intermediate geothermal water temperature at $T_{gw,in}$=100℃.

The ratio of the exergetic efficiency to the total thermal conductance is chosen as the evaluation indicator ($\eta_{ex}/((KA)_{total})$. The numerator, η_{ex}, reflects the system earnings, and the denominator, $(KA)_{total}$, reflexes the system cost. Moreover, for the convenience of simplifying the comparison between SDCORC and ORC, the ratio $(\eta_{ex}/((KA)_{total})_{SDCORC}/\eta_{ex}/((KA)_{total})_{ORC})$ is chosen as the objective function. The dimensionless ratio $(\eta_{ex}/((KA)_{total})_{SDCORC}/\eta_{ex}/((KA)_{total})_{ORC})$ versus the GWIT is depicted in Figure 7. Obviously, as indicated in the figure, $(\eta_{ex}/((KA)_{total})_{SDCORC}/\eta_{ex}/((KA)_{total})_{ORC})$ first increases and then decreases with T_{eva}. The maximal values of $(\eta_{ex}/((KA)_{total})_{SDCORC}/\eta_{ex}/((KA)_{total})_{ORC})$ is 1.096. $(\eta_{ex}/((KA)_{total})_{SDCORC}/\eta_{ex}/((KA)_{total})_{ORC})$ always surpasses 1.000, illustrating that the SDCORC evidently exceeds the ORC.

From the above-mentioned analysis, the SDCORC enhances the net power output, which is at the expense of a larger total thermal conductance requirement. The extent of improvement is proportional to the GWIT, and this is due to that the SDCORC pumps a portion of the saturated liquid in the low-pressure stage evaporator to the high-pressure stage evaporator, and thus the SDCORC improves the matching between the heat source and the working fluid in the evaporator. Therefore, the SDCORC manifests more excellent systematic performances, which can be popularized in engineering applications. In actual, it should be specially pointed out that the SDCORC absorbs a portion of heat from the lower temperature range to preheat the working fluid in the low-pressure stage evaporator, which is the reason for that the SDCORC exceeds the ORC.

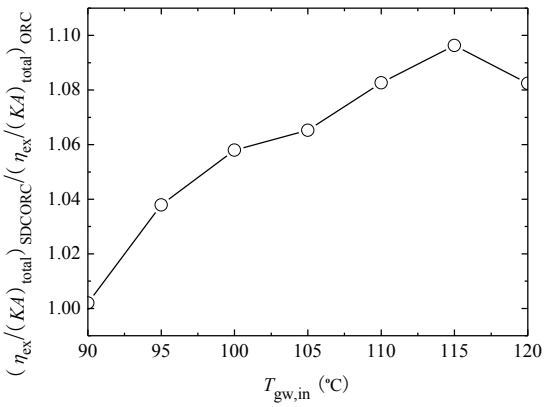

Figure 7: Ratio of the exergetic efficiency to the total thermal conductance with geothermal water inlet temperature.

5. CONCLUSIONS

The ORC is promising in energy recovery for low- and medium-grade heat sources, but the evaporator contributes the most to the total irreversible loss. This study proposes the segmented utilization of the heat source, and the series double cascade-evaporating technology has been adopted to replace the single evaporating. The SDCORC is presented to improve the matching between the heat source and the working fluid using R245fa, thereby enhancing the systematic performance. The system parameters are calculated and optimized. The main conclusions that can be drawn from the present study may be summarized as follows:

(1) The SDCORC segments the heat source in two ranges, improving the matching between heat source and working fluid.

(2) There exists an optimal IGWT and evaporating temperatures for the SDCORC to maximize the net power output.

(3) The SDCORC can enhance the net power output and the growth rate differs with GWIT and IGWT, but the total thermal conductance is almost the same with the ORC, moreover, the SDCORC is more preferable for higher GWITs.

(5) The SDCORC presents excellent systematic performance, which should be popularized in engineering applications.

ACKNOWLEDGMRNTS

The authors gratefully acknowledge the financial support provided by the National High Technology Research and Development Program of China (863 Program) (Grant No. 2012AA053001).

REFERENCES

Bianchi, M., and De Pascale, A.: Bottoming cycles for electric energy generation: parametric investigation of available and innovative solutions for the exploitation of low and medium temperature heat sources, *Applied Energy*, **88**, (2011), 1500-1509.

Calm, J.M., Hourahan, G.C.: Refrigerant data update, *Heat/Pip/Air Cond Eng*, **79**, (2007), 50-64.

DiPippo, R.: Second law assessment of binary plants generating power from low-temperature geothermal fluids, *Geothermics*, **33**, (2004), 565-86.

Eurostat, Electricity prices for household consumers; 2013. <http:// www.epp.eurostat.ec.europa.eu>.

Fernández, F.J., Prieto, M.M., and Suárez, I.: Thermodynamic analysis of high-temperature regenerative organic Rankine cycle using siloxanes as working fluids, *Energy*, **36**, (2011), 5239-5249.

Fiaschi, D., Manfrida, G., and Maraschiello, F.: Thermo-fluid dynamics preliminary design of turbo-expanders for ORC cycles, *Applied Energy*, **97**, (2012), 601-608.

Franco, A.: Power production from a moderate temperature geothermal resource with regenerative Organic Rankine Cycles, *Energy and Sustainable Development*, **15**, (2011), 411-419.

Invernizzi, C., Iora, P., and Silva, P.: Bottoming micro-Rankine cycles for micro-gas turbines, *Applied Thermal Engineering*, **27**, (2007), 100-110.

Kanoglu, M.: Exergy analysis of dual-level binary geothermal power plant, *Geothermics*, **31**, (2002), 709-724.

Li, M.Q., Wang, J.F., He, W.F., Gao, L., Wang, B., Ma, S.L., and Dai,Y.P.: Construction of preliminary test of a low-temperature regenerative organic Rankine cycle (ORC) using R123, *Renewable Energy*, **57**, (2013), 216-222.

Li, T.L., Zhu, J.L., Xin, S.L., and Zhang, W.: A novel geothermal system combined power generation, gathering heat tracing, heating/domestic hot water and oil recovery in an oilfield, *Geothermics*, **51**, (2014), 388-396.

Li, T.L., Zhu, J.L., and Zhang, W.: Implementation of PDORC (parallel double-evaporator organic Rankine cycle) to enhance power output in oilfield, *Energy*, **68**, (2014), 680-687.

Li, T.L., Zhu, J.L., and Zhang, W.: Cascade utilization of low temperature geothermal water in oilfield combined power generation. gathering heat tracing and oil recovery, *Applied Thermal Engineering*, **40**, (2012), 27-35.

Li, T.L., Zhu, J.L., and Zhang, W.: Comparative analysis of series and parallel geothermal systems combined power, heat and oil recovery in oilfield, *Applied Thermal Engineering*, **50**, (2013),1132-1141.

Li, T.L., Zhu, J.L., and Zhang, W. and Li, J.: Thermodynamic optimization of a neoteric geothermal poly-generation system in an oilfield, *International Journal of Energy Research*, **37**, (2013), 1939-1951.

Li, T.L., Zhu, J.L., and Zhang, W.: Performance analysis and improvement of geothermal binary cycle power plant in oilfield, *Journal of Central South University*, **20**, (2013), 457-465.

Liu, B., Rivière, P., Coquelet, C., Gicquel, R., David, F.: Investigation of a two stage Rankine cycle for electric power plants, *Applied Energy*, **100**, (2012), 285-294.

Kosmadakis, G., Manolakos, D., and Papadakis, G.: Parametric theoretical study of a two-stage solar organic Rankine cycle for RO desalination, *Renewable Energy*, **35**, 2010, 989-996.

Kosmadakis, G., Manolakos, D., Kyritsis, S., and Papadakis, G.: Economic assessment of a two-stage solar organic Rankine cycle for reverse osmosis desalination, *Renewable Energy*, **34**, (2009), 1579-1586.

Macchi, E., and Perdichizzi, A.: Efficiency prediction for axial-flow turbines operating with non conventional fluids, Trans ASME, Journal of Engineering Power, **103**, (1981), 718-724.

Mago, P.J., Chamra, L.M., Srinivasan, K., and Somayaji, S.: An examination of regenerative organic Rankine cycles using dry fluids, *Applied Thermal Engineering*, **28**, (2008), 998-1007.

Mago, P.J., Srinivasan, K.K., Chamra, L.M., et al: An examination of exergy destruction in organic Rankine cycles, *International Journal of Energy Research*, **32**, (2008), 926-938.

Mohammadkhani, F., Shokati, N., Mahmoudi, S.M.S., Yari, M., and Rosen, M.A.: Exergoeconomic assessment and parametric study of a Gas-Turbine-Modular Helium Reactor combined with two Organic Rankine Cycles, *Energy*, **65**, (2014), 533-543.

Pei, G., Li, J., and Ji, J.: Analysis of low temperature solar thermal electric generation using regenerative Organic Rankine Cycle, *Applied Thermal Engineering*, **30,** (2010), 998-1004.

Quoilin, S., and Orosz, M., Hemond, H., and Lemort, V.: Performance and design optimization of a low-cost solar organic Rankine cycle for remote power generation, *Solar Energy*, **85**, (2011), 955-966.

Roy, J.P., Misra, A.: Parametric optimization and performance analysis of a regenerative organic Rankine cycle using R-123 for waste heat recovery, *Energy*, **39**, (2012), 227-235.

Saleh, B., Koglbauer, G., Wendland, M., and Fischer, J.: Working fluids for low temperature organic Rankine cycles, *Energy*, **32**, (2007), 1210-1221.

Shengjun, Z., Huaixin, W., and Tao, G.: Performance comparison and parametric optimization of subcritical Organic Rankine Cycle (ORC) and transcritical power cycle system for low-temperature geothermal power generation, *Applied Energy*, **88**, (2011), 2740-2754.

Shu, G.Q., Liu, L.N., Tian, H., Wei, H.Q., and Liang, Y.C.: Analysis of regenerative dual-loop organic Rankine cycles (DORCs) used in engine waste heat recovery, *Energy Conversion and Management*, **76**, (2013), 234-423.

Shu, G.Q., Liu, L.N., Tian, H., Wei, H.Q., and Xu, X.F.: Performance comparison and working fluid analysis of subcritical and transcritical dual-loop organic Rankine cycle (DORC) used in engine waste heat recovery, *Energy Conversion and Management*, **74**, (2013), 35-43.

Shu, G.Q., Liu, L.N., Tian, H., Wei, H.Q., and Yu, G.P.: Pearametric and working fluid analysis of a dual-loop organic Rankine cycle (DORC) used in engine waste heat recovery, *Applied Energy*, **113**, (2014) 1188-1198.

Sun, F.M., Ikegami, Y., Jia, B.J., and Arima, H.: Optimization design and exergy analysis of organic rankine cycle in ocean thermal energy conversion, *Applied Ocean Research*, **35**, (2012), 38-46.

Toffolo, A., Lazzaretto, A., Manente, G., and Paci, M.: A multi-criteria approach for the optimal selection of working fluid and design parameters in Organic Rankine Cycle systems, *Applied Energy*, **121**, (2014), 219-232.

U.S Energy Information Administration, Average retail price of electricity to ultimate customers. <http://www.eia.gov>.

U.S. Energy Information Administration, International energy outlook 2011, Washington, DC; 2011.

Wang, E.H., Zhang, H.G., Zhao, Y., Fan, B.Y., Wu, Y.T., and Wu, Q.H.: Performance analysis of a novel system combining a dual loop organic Rankine cycle (ORC) with a gasoline engine, *Energy*, **43**, (2012), 385-395.

Xi, H., Li, M.J., Xu, C., and He, Y.L.: Parametric optimization of regenerative organic Rankine cycle (ORC) for low grade waste heat recovery using genetic algorithm, *Energy*, **58**, (2013), 473-482.

Yang, F.B/, Dong, X.R., Zhang, H.G., et al.: Performance analysis of waste heat recovery with a dual loop organic Rankine cycle (ORC) system for diesel engine under various operating conditions, *Energy Conversion and Management*, 80, (2014), 243-255.

Zhang, J.H., Zhou, Y.L., Li, J., Hou, G.L., and Fang, F.: Generalized predictive control applied in waste heat recovery power plants, *Applied Energy*, **102**, (2013), 320-326.

Zhang, H.G., Wang, E.H., and Fan, B.Y.: A performance analysis of a novel system of a dual loop organic Rankine cycle (ORC) with a light-duty diesel engine, *Applied Energy*, **102**, (2013), 1504-1513.